

8-20-1993

Characterization of the Complex Sulfide Ore of Sotiel (Spain) by Scanning Electron Microscopy and Electron Microprobe Analysis

Giuseppe Bonifazi

Universita' degli Studi di Roma "LA SAPIENZA"

Roberto Gorga

C.N.R.

Follow this and additional works at: <https://digitalcommons.usu.edu/microscopy>



Part of the [Biology Commons](#)

Recommended Citation

Bonifazi, Giuseppe and Gorga, Roberto (1993) "Characterization of the Complex Sulfide Ore of Sotiel (Spain) by Scanning Electron Microscopy and Electron Microprobe Analysis," *Scanning Microscopy*. Vol. 7 : No. 4 , Article 7.

Available at: <https://digitalcommons.usu.edu/microscopy/vol7/iss4/7>

This Article is brought to you for free and open access by the Western Dairy Center at DigitalCommons@USU. It has been accepted for inclusion in Scanning Microscopy by an authorized administrator of DigitalCommons@USU. For more information, please contact digitalcommons@usu.edu.



CHARACTERIZATION OF THE COMPLEX SULFIDE ORE OF SOTIEL (SPAIN) BY SCANNING ELECTRON MICROSCOPY AND ELECTRON MICROPROBE ANALYSIS

Giuseppe Bonifazi*, Roberto Gorga¹

Dipartimento di Ingegneria Chimica, dei Materiali, delle Materie Prime e Metallurgia
Universita' degli Studi di Roma "LA SAPIENZA", Via Eudossiana 18, 00184 Roma, Italy

¹Istituto per il Trattamento dei Minerali, C.N.R., Via Bolognola 7, 00138 Roma, Italy

(Received for publication February 2, 1993, and in revised form August 20, 1993)

Abstract

This study complements a more exhaustive examination on the complex sulfide mineralization of Sotiel, (Spain), by optical microscopy and multispectral digital analysis of images. Electron microscopy analyses were carried out to document specific associations which are difficult to detect with conventional optical microscopy. This study utilizes the application of digital techniques to image processing, in an attempt to define microstructural and microtextural characteristics of the ore, since they play an important role in the subsequent beneficiation operations (i.e., flotation).

Scientific and economic information bound to complex metallogenic phenomenology and referred to particular paragenetic scenes was acquired by the study in detail of inclusions of main mineralogical species such as pyrite, sphalerite, galena, chalcopyrite combined with quartzose-carbonate-micaceous gangues and a particular silico-marly "slate".

Scanning electron microscopy and optical microscopy observations and image analysis were used to characterize species of metallic and non-metallic submicroscopic inclusions.

Key words: Scanning electron microscopy, complex sulfide ore, texture, structure, beneficiation.

* Address for correspondence:

Giuseppe Bonifazi
Dipartimento di Ingegneria Chimica, dei Materiali,
delle Materie Prime e Metallurgia
Via Eudossiana 18,
00184 Roma,
Italy

Phone: (39.6) 44585-925

FAX: (39.6) 44585-618

Introduction

The lead and zinc mixed sulfide mineralizations are of great industrial interest since most lead and zinc are derived from this kind of deposits. This abundance of ores is not matched by their quality after industrial separation of sphalerite (Zns) and galena (Pbs) from gangue (Gorga, 1989). These mineral associations show textural and structural characteristics which make use of beneficiation techniques, based on traditional procedures (comminution, gravimetric separation and flotation), very difficult. For these reasons adequate research techniques aimed at detecting microinclusions and/or replacements inside or on the surface of species considered pure are necessary. This information can only be detected at micrometer scale by means of scanning electron microscopy (SEM) and X-ray microanalysis (XRMA) techniques (Bonifazi and Massacci, 1986; Bonifazi and Gorga, 1993, submitted for publication; Petruk, 1990).

This present work is the result of a study carried out to make a complete characterization from the mineral-petrographic and mineral-chemical point of view of Sotiel (Spain) mineralization. Therefore, this information is an essential premise to a rational assessment to improve the recovery and grades of monomineral concentrates of pyrite (FeS₂), sphalerite (ZnS), galena (PbS), chalcopyrite (CuFeS₂) together with other possible metallic elements which are interesting from the economic point of view, such as silver, or harmful elements, such as arsenic and/or antimony.

The results obtained from a parallel study (Bonifazi and Gorga, 1993, submitted) of the ore showed great variability in chemical and textural parameters. Those results pointed to a need for a more exhaustive study utilizing different analytical techniques:

- mineralogical study through optical microscope with natural and polarized reflected light;
- elementary chemical analysis;
- microstructural and microanalytical study through SEM for backscattered and secondary electrons, and electron probe microanalyzer;
- image analysis.

Table 1. Chemical analyses of elements and silver in trace, carried out by atomic absorption (Perkin Elmer ICP 6000) on five samples representative of the mineral coming from the Sotiel Ore.

Element (%)	Ore Samples				
	SLF1	SLF2	SLF3	SLF4	SLF5
Zn	5.06	4.24	4.55	4.60	4.80
Pb	2.10	1.99	2.02	2.04	1.91
Cu	0.76	0.67	0.68	0.66	0.80
Total	7.92	6.90	6.45	6.30	7.51
Element (ppm)					
Ag	34.99	46.89	44.66	45.00	46.00

The complex of these procedures, with their analogical and digital integration, allowed us to make a precise assessment of the balance and degree of liberation of mineral phases containing those metallic elements which are useful or harmful from the economic point of view (Bonifazi and Massacci, 1988, 1989; Petruk, 1986, 1988). The digital information allowed us to create data bases of great historical interest and baseline information.

Materials and Methods

Materials

The pyrite-cupriferous deposit of Sotiel is a few kilometers from Calanas in the minerogenetic subprovince of Huelva (Spain); it is characterized northwards by the spurs of Western reliefs of Sierra Morena and southwards from Spanish Atlantic coasts (Fernandez, 1975). The metallogenetic province was already known at the time of Phoenicians while the deposit of Sotiel supposedly was the object of mining during the Roman dominion.

The structural aspect of "Faja Piritica Iberica" is characterized by a slight metamorphism with at least four folded episodes. These correspond to a geological period included between the Devonian and the beginning of Carboniferous of contemporaneous or previous grounds to the principal phase of the Hercinian orogeny (Apps, 1961; Bard, 1965; Delcey, 1970; Febrel, 1967; Febrel-Moliner, 1966; Garcia-Palomero, 1974; Lecolle, 1970, 1971, 1972; Lecolle and Roger, 1973; Rambaud, 1969; Schermerhorn, 1971; Soler, 1971).

The deposit of Sotiel is made up of a single principal ore body with foliated-lenticular geometry, with an average thickness of around 50 meters. The metalliferous horizon presumably developed in a volcanic-sedimentary complex in a metamorphosed environment made up of wall-black slates and pyroclastic products showing interposed roof to a powerful formation of vulcanite (Arnold and Soler, 1973). The present theories (Apps, 1961; Kinkel, 1962) suggest that the structure was involved by high extrusive-sedimentary activity in a submarine floor similar to that observed in the recent submarine geothermal fields located in numerous points adjoining those countries which face the Mediterranean Sea.

Table 2. Chemical analyses (% content as elements), carried out by electron microscopy/microprobe analysis (JEOL JSM-50A) on the main minerals in the Sotiel ore. The values represent means relative to numerous analyses performed on five samples of the same ore.**Table 2A.** Pyrite Species.

Element (%)	Massive pyrite	Schistose pyrite
Fe	44.12	46.46
Zn	-	-
Pb	-	-
Cu	0.11	-
Ag	0.04	-
Au	0.09	trace
S	53.39	52.12
As	0.46	0.25
Cd	-	-
Co	0.23	-
Sb	-	0.07
Mn	-	-
Bi	-	0.17
Total	98.44	99.27

Table 2B. Other minerals.

Element (%)	Mineral Species					
	sp	gn	ccp	apy	gdm	ttr
Fe	4.22	-	29.51	33.65	22.99	2.21
Zn	67.55	-	0.41	0.55	-	-
Pb	-	86.01	3.83	1.21	0.05	1.02
Cu	0.16	-	31.88	0.23	0.07	41.22
Ag	-	0.17	-	0.10	0.15	0.56
Au	-	0.09	-	0.07	0.06	-
S	28.04	11.58	33.78	18.36	21.53	24.38
As	-	-	-	46.83	1.03	-
Cd	-	-	-	0.42	-	4.03
Co	0.07	-	0.02	0.25	-	-
Sb	-	-	-	-	52.75	26.51
Mn	-	-	-	-	-	-
Bi	-	-	-	-	0.25	-
Total	100.04	98.65	99.43	101.67	98.88	99.93

sp: sphalerite; gn: galena; ccp: chalcopyrite; apy: arsenopyrite; gdm: gudmundite; ttr: tetrahedrite.

The metalliferous body, 950 meters long, has a reserves estimated around 59×10^6 tons of crude containing 4.2% Zn, 1.6% Pb, 0.6% Cu and 30 grams/ton of Ag.

The experimental work was carried out on a material taken from a 120 kg sample coming from the deposit. This sample, provided by the agency "Minas de Almagrera", was subjected to a crushing process resulting in a product with sizes lower than 10 mm. A sampling was carried out on this material which gave an average

Characterization of Complex Sulfide Ores

Table 3. Main microscopic and submicroscopic inclusions of minerals (useful elements to be recovered and harmful elements to be separated) detected in the Sotiel ore. The study has been carried out by optical reflected light microscopy (JENAPOL-U), scanning electron microscopy (Zeiss DSM-960), electron microprobe (JEOL JSM-50A), and systems of multispectral image analysis.

Host minerals	Useful elements	Included minerals	Harmful elements
Pyrite	S, Co, Ag, Au	marcasite, melnikovite, magnetite	Zn, Pb, As, Sb
Sphalerite	Zn	galena, calchopirite, arsenopyrite	Fe, Cu, Sb
Galena	Pb, Ag	tetrahedrite	As, Sb
Chalcopyrite	Cu	sphalerite, galena	Zn, Pb, Fe, As
Arsenopyrite	Ag	sphalerite, galena, calchopirite	As
Tetrahedrite	Ag		Sb, As
Gudmundite	Ag		As, Bi

grain weight of about 250 grams. It was washed with distilled water and dried in the furnace at 50°C.

Optical microscopy

The sample was placed in a special holder containing an epoxy resin ("Castolite") with a catalytic agent (in the proportions four to one) and was left to harden at 50°C. The sample was then cut, and also thin sections (3-4 mm) were prepared; these samples and sections were polished using standard petrographic procedures. The final polishing was carried out using ultra-fine alumina particles of 5 μm .

The preliminary study on specimens was carried out using a JENAPOL-U optical microscope for primary characterization and structural, textural and morphological characteristics of the minerals. This study was insufficient for some samples, because it gave very little useful information for the definition and setting up of research strategies for SEM and XRMA. In some case, even high magnification (using special oil dipping objectives) was insufficient to interpret some submicroscopic inclusions.

Characterization

The detailed morphological study of the crude ore was carried out through optical reflected light microscopy, SEM and digital image analysis. In addition, XRMA was performed on the points and areas of interest which were recognized by optical and/or electron microscopy. An home made modular system, created by assembling different specific hardware, was employed to acquire, handle and process digital image data from optical microscope and SEM.

This investigation started with research aimed at defining minero-petrographic and chemical characteristics of the ore; this information is an important prerequisite to study the concentration of pyrite (FeS_2), sphalerite (ZnS), galena (PbS), chalcopyrite (CuFeS_2) with other economically important metallic elements. Since the great abundance of minerals present are opaque, this study was carried out mainly under reflected light (Figures 1-5). In some case, observations of thin sections were useful in determining the presence of gangue minerals with carbonate-quartzose composition.

Chemical analyses Prior to the studies aimed at defining the textural, structural, and compositional characteristics between the different phases, chemical analyses were performed to assess the elementary composition of the ore. Only analyses of Pb, Zn, Cu and Ag were carried out, since these elements are sufficient to define a subsequent optimization strategy of recovery of these metals in the beneficiation studies. Chemical analysis was performed on five samples, designated, SLF1, ..., SLF5. The results of chemical analysis are presented in Table 1. From these chemical analysis, we conclude:

a) There are no significant differences in the analytical data of the five samples with regards to Zn, Pb, Cu, and Ag. These can be considered equivalent.

b) Apart from the large amount of Fe (not analyzed) in pyrite (FeS_2), chalcopyrite (CuFeS_2), and other accessory minerals such as marcasite (FeS_2), melnikovite (crystallized FeS_2 gel) and magnetite (FeFe_2O_4), Zn present in sphalerite (ZnS) is the principal constituent.

c) The amount of sphalerite (ZnS) in five samples was: SLF1 = 7.54%; SLF2 = 6.76%; SLF3 = 6.78%; SLF4 = 6.85%; and SLF5 = 7.15%. Galena (PbS) varied from 2.42% to 2.21%; while chalcopyrite (CuFeS_2) ranged from 2.30% to 1.90%.

d) Silver in moderate amounts (~ 45 ppm) was present in all samples. However, the contents of Ag can be considerable when compared to the percentages of galena or some accessory minerals. In fact, in addition to galena, minerals containing Ag, as shown in the following analysis through XRMA, are tetrahedrite ($\text{Cu}_3\text{Sb}_3\text{S}_4$), gudmundite (FeSbS), arsenopyrite (FeAsS).

Scanning electron microscopic examinations

The specimens for SEM investigation were the same as those used for with optical microscopy; identical areas were studied by optical microscopy, SEM and XRMA. SEM examinations were carried out using a DSM-960 Zeiss SEM which was also equipped for energy dispersive X-ray microanalysis. Qualitative X-ray analyses were performed on SEM only to obtain morphological and morphometrical characteristics of microinclusions which were difficult to recognize by optical microscopy. In some cases, mineral phases constituting microinclusions were determined.

The atomic number contrast in backscattered electron (BSE) images on SEM permitted qualitative minerochemical composition determination. Using the BSE images, following minerals could be recognized: pyrite (FeS_2), sphalerite (ZnS), argentic galena (PbS), chalcopyrite (CuFeS_2), arsenopyrite (FeAsS), argentic gudmundite (FeSbS), magnetite (FeFe_2O_4), carbonate and/or quartzose gangue (Figures 6-11).

Legends for Figures 1-5 (on the facing page 1185).

Figure 1. Sotiel complex sulfide ore, as mined (optical reflected light). Granular structure and typical texture of mineral with poor porosity and intergranular vacuum generally filled with interstitial minerals. The diffusion of microscopic and submicroscopic inclusions is determined by the presence of granular cribriform pyrite (FeS_2) (**py**) with frequent trend to idiomorphism associated and/or included in sphalerite (ZnS) (**sp**), a light gray variety in Fe with inner reflexes. In sphalerite, in addition to hypidiomorphic pyrite, argentic galena (PbS) (**gn**) interstitial aggregates can be distinguished. The dark zones are due not only to blowholes but also to the presence of magnetite (FeFe_2O_4) and carbonate gangue minerals (ankeritic dolomite). From the image it is possible to detect the extreme textural complexity and difficulties of survey through optical microscopy of the structure and size of microinclusions present in the mineral phases of interest. (Polished section).

Figure 2. Sotiel complex sulfide ore, as mined (optical reflected light). Eudral crystal of cribriform pyrite (FeS_2) (**py**) developed in a blowhole with submicroscopic inclusions of sphalerite (ZnS) (**sp**). (**dol-ank**): dolomite-ankerite gangue. The distribution of submicroscopic inclusions of sphalerite inside the crystal of pyrite is reported. The different regions constituted by sphalerite are "labeled" according to the recognition sequence followed by the algorithm (from up-right to bottom-left). Only regions presenting an area constituted of more than 10 pixels are displayed. (Polished section).

Number of sphalerite (ZnS) domains recognized and identified inside the pyrite (FeS_2) crystal (number of domains: 35).

Measure	Min	Max	Range	Sum	Mean	S.D.
Area	28	1066	1038	4813	137.5	196.7
Perimeter	17	190	173	1928	55.1	39.2
Roundness	1	5	4	75	2.1	1.3
Maj.Ax.	7	56	49	655	19.2	11.6
Min.Ax.	5	25	20	296	8.5	4.7

The *Area* and the *Perimeter* are expressed in pixels (1 pixel = 1.05 μm). S.D. = Standard deviation.

Figure 3. Sotiel complex sulfide ore, as mined (optical reflected light). Eudral crystal of arsenopyrite (FeAsS) (**apy**) and cribriform subautomorphic pyrite (FeS_2) (**py**) (above, right) with numerous inclusions of sphalerite (ZnS) (**sp**) (gray) included together with chalcopyrite (CuFeS_2) (**ccp**). As in Figure 2, the different regions constituted by sphalerite are "labeled" according to the recognition sequence followed by the algorithm. Only regions presenting an area constituted of more than 10 pixels are displayed. (Polished section).

Number of sphalerite (ZnS) domains recognized and identified inside the arsenopyrite (FeAsS) crystal (number of domains = 16).

Measure	Min	Max	Range	Sum	Mean	S.D.
Area	22	856	834	3859	241.2	234.5
Perimeter	22	381	359	1844	115.3	92.9
Roundness	2	13	12	78	4.9	3.1
Maj.Ax.	6	68	62	434	27.2	15.7
Min.Ax.	5	24	19	188	11.8	6.0

The *Area* and the *Perimeter* are expressed in pixels (1 pixel = 1.05 μm). S.D. = Standard deviation.

Figure 4. Sotiel complex sulfide ore, as mined (optical reflected light). Marmatitic sphalerite (ZnS) (**sp**) with heterogranular inclusions of cribriform pyrite (FeS_2) (**py**) cord exsolutions of chalcopyrite (CuFeS_2) (**ccp**) interrupted by magnetite (FeFe_2O_4) (**mag**). Chalcopyrite shows ultrafine inclusions of sphalerite. The blackish aggregates represent mineral of gangue and blowholes. The different regions constituted by pyrite are shown and "labeled". Only regions presenting an area constituted of more than 10 pixels are displayed. (Polished section).

Number of Pyrite (FeS_2) domains recognized and identified (number of Domains = 101).

Measure	Min	Max	Range	Sum	Mean	S.D.
Area	21	1075	1054	18261	180.8	201.9
Perimeter	13	413	40	7181	71.1	67.2
Roundness	1	15	14	243	2.4	2.1
Maj.Ax.	5	61	56	2000	19.8	11.9
Min.Ax.	5	33	28	1100	10.9	6.0

The *Area* and the *Perimeter* are expressed in pixels (1 pixel = 1.05 μm). S.D. = Standard deviation.

Figure 5. Sotiel complex sulfide ore, as mined (optical reflected light). Exsolutions of chalcopyrite (CuFeS_2) (**ccp**) in an aggregate with radiated structure of marcasite-melnikovite (**mrc**), touching marmatitic sphalerite (ZnS) (**sp**) where inclusions of cribriform pyrite (FeS_2) (**py**) and galena (**gn**) are found. (Polished section).

Characterization of Complex Sulfide Ores

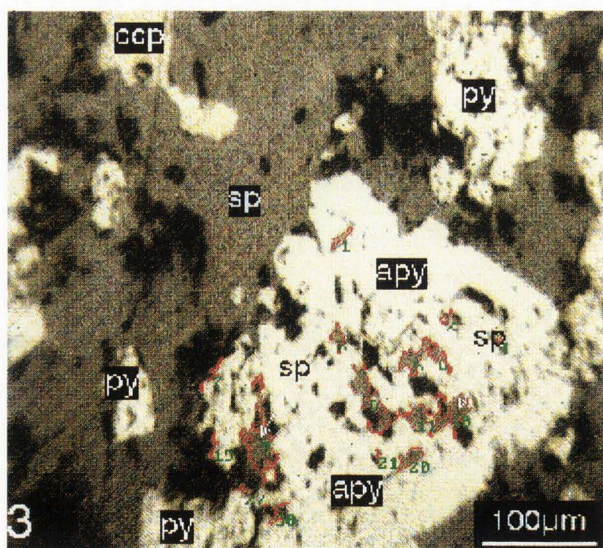
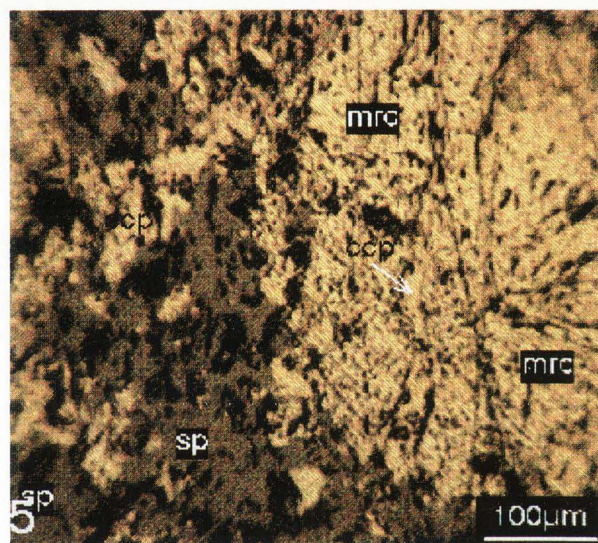
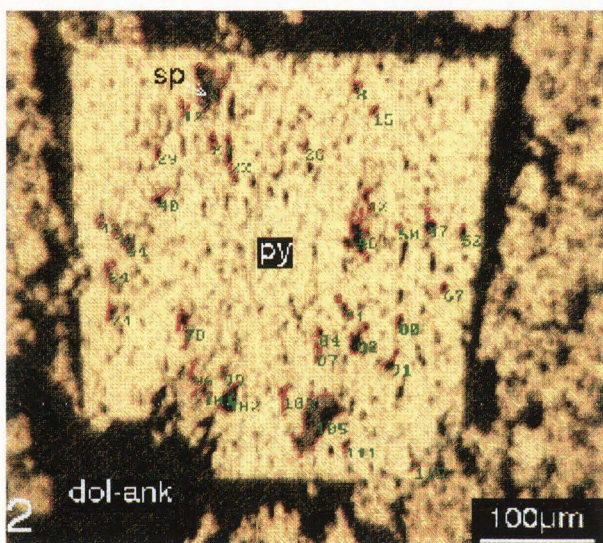
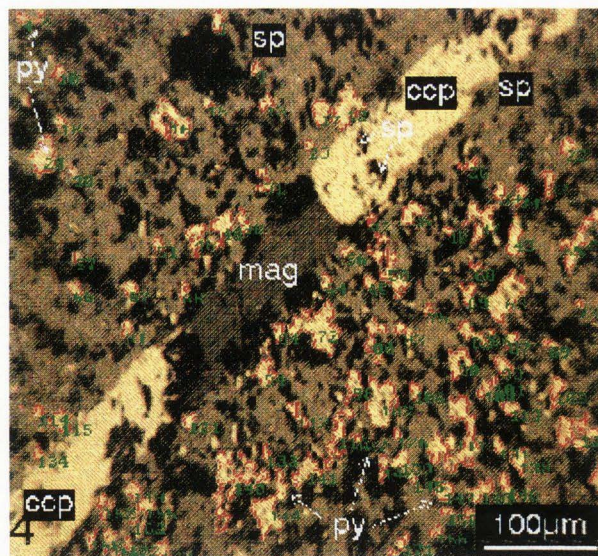
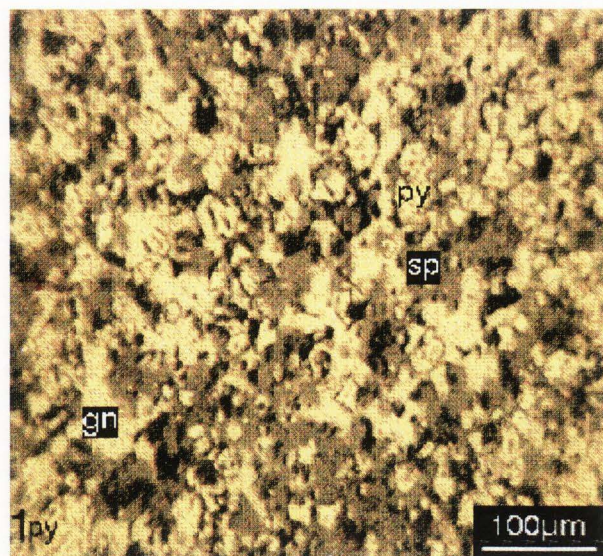


Table 4. Experimental conditions for XRMA (using EDS Link System AN 10000-85S at 15 kV and a beam current of 2×10^{-9} A; number of analyzed points = 60).

Element	Wavelength	Reference Material
Fe	K α	pyrite
Zn	K α	element
Pb	K α	Pb metal
Cu	K α	element
Ag	L α	element
Au	M α	element
S	K α	pyrite
As	L α	element
Cd	L α	element
Co	K α	element
Sb	L α	element
Mn	K α	element
Bi	M α	element

X-ray microanalyses Electron probe X-ray microanalysis was essential in determining the quantitative composition of various minerals and microinclusions present in the ore samples. Table 2 presents results for elements occurring in the "as mined" ores in the Sotiel deposit. XRMA allowed us to detect microelements present in pure mineralogical phases and microstructural interpretation of the same species. The XRMA results, relating to microtextures present in zones of intergranular contact, proved very important to the setting up of the subsequent beneficiation process (Table 3).

The XRMA and mineralogical results are summarized below (Tables 2 and 3):

a) Pyrite (FeS_2) is present in all lithologic types examined but it has different structures: in samples characterized by massive clastic rock (Fig. 1) pyrite appears as idiomorphic crystals (Fig. 2) and grains in sphalerite (Fig. 4); in the schistose lithologic types, it is possible to recognize isooriented spheroidal forms floating in a microcrystalline matrix characteristics of a quartzose slate.

b) Iron (average content typically more than 4%) is homogeneously distributed in sphalerite (ZnS).

c) The amount of silver present within galena (PbS), arsenopyrite (FeAsS), gudmundite (FeSbS), tetrahedrite ($\text{Cu}_3\text{Sb}_3\text{S}_4$) ranged from 0.17 to 0.56%.

d) The mineralogical phases containing As and Sb are pyrite (FeS_2), arsenopyrite, gudmundite and tetrahedrite, while Bi is distinguishable only in pyrite and tetrahedrite.

A JEOL JXA GSM 50A was used to perform the X-ray microanalyses. Table 4 lists the experimental conditions.

Results

These studies show that the ore is composed of two structural types:

- The first structure has black color, schistose characteristics, and occurs without vacuolar micro-blowholes possessing good mechanical strength. It shows highly anisotropic texture with ultrafine grain-size with framboid, spheroidal structure made up of pyrite and other microinclusions (Fig. 1). Rock seems weakly metamorphosed with silico-marly composition and carbon-ochraceous matter. On the basis of textural evidence and XRMA results, it is possible to state that the this structure has the same chemical composition as the semimetamorphic arenaceous-pelitic derivatives of siltitic schists, typical of some "slates" (Table 2).

- The second structure (Figures 2 and 3), gray in color, is lithified with micro-blow-holes ranging from few μm to ten μm , and has lower mechanical strength in comparison with the previous lithologic type. It shows subautomorphic heterogranular clastic structure, anisotropic texture with fine grain-size characterized by sulfuric compounds of Fe, Zn, Pb, Cu with submicroscopic and/or microscopic inclusions of the pyrite (FeS_2), sphalerite (ZnS), Ag-galena (PbS) and, subordinately, species such as arsenopyrite (FeAsS), Ag-Au

Legends for Figures 6a, 7a, 8a, 9a, 10a, and 11a on facing page 1187 (the corresponding Figures 6b, 7b, 8b, 9b, 10b, and 11b are on color plate at page 1188, with their legends on its facing page 1189; and the corresponding Figures 7c, 8c, 9c and 9d are on page 1190).

Figure 6a. Sotiel complex sulfide ore, as mined (back-scattered electron image, BEI). At center: automorphic crystal of gudmundite.

Figure 7a. Sotiel complex sulfide ore, as mined (BEI); magnified view of area W1 in Figure 6b. Granular aggregates of sphalerite (ZnS) (**sp**) (gray) separated by two aggregates of magnetite (FeFe_2O_4) (**mag**) (black) rich in blowholes often filled with magnetite and carbonate gangue (dolomite-ankerite). Sphalerite shows a variety with inner dark reflexes with grains and granular large-size aggregates (up to 100 μm) and rich in inclusions of arsenopyrite (FeAsS) (**apy**) with idiomorphic behavior. Sometimes, it is possible to detect interstitial aggregates of argentic galena (PbS) (**gn**) (white). At center: an idiomorphic crystal of argentic gudmundite (FeSbS) (**gdm**) (see Fig. 7b).

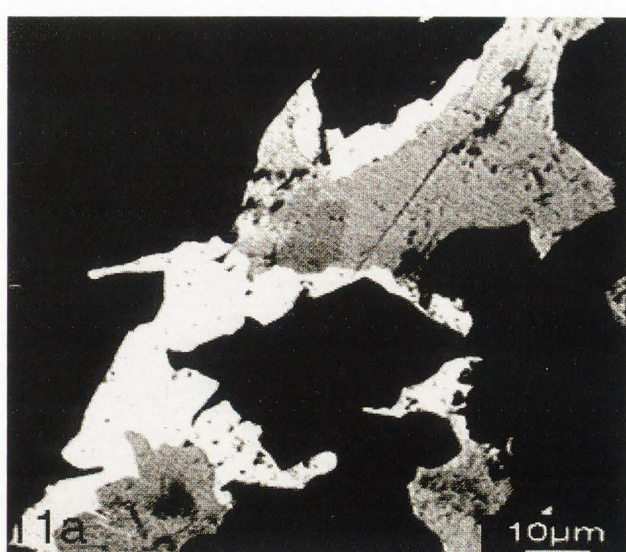
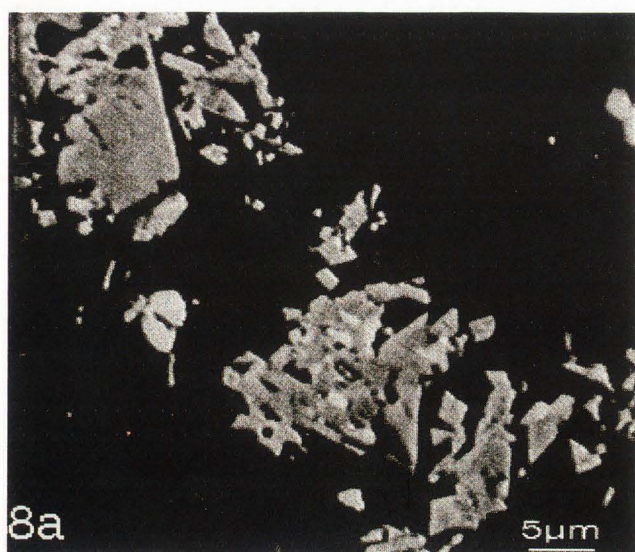
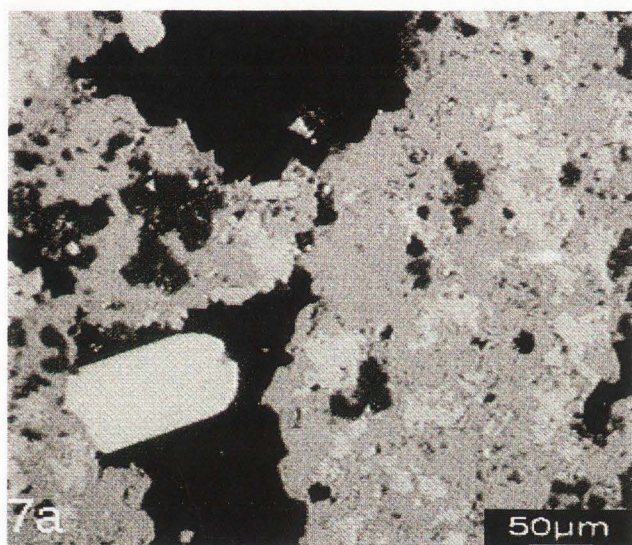
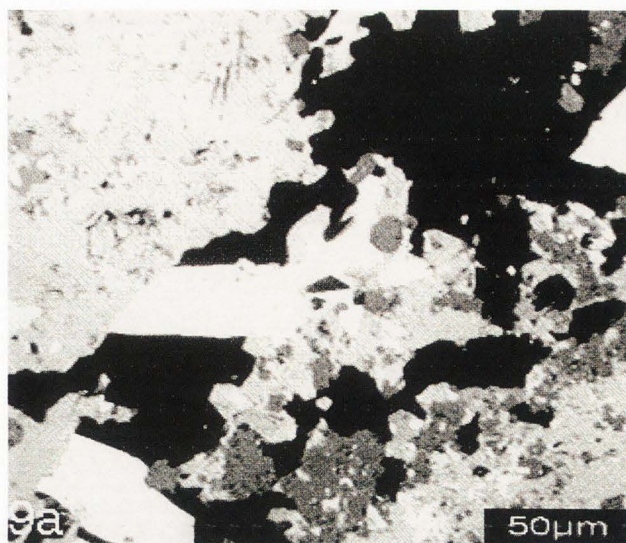
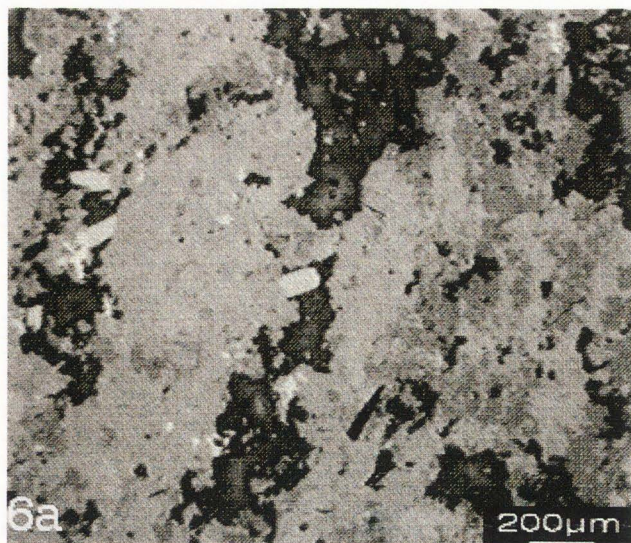
Figure 8a. Sotiel complex sulfide ore, as mined (BEI). Note the submicroscopic inclusions of arsenopyrite (FeAsS) (**apy**) in idiomorphic or subautomorphic crystals with submicroscopic interstitial aggregates of argentic galena (PbS) (**gn**) (see Fig. 8b).

Figure 9a. Sotiel complex sulfide ore, as mined (BEI), magnified view of area W2 in Figure 6b. It is possible to see automorphic crystals of arsenopyrite (FeAsS) (**apy**) grown together in the base on sphalerite (ZnS) (**sp**) (gray) and included in magnetite (FeFe_2O_4) (**mgm**) (black). The white fringes associated with the crystal of gudmundite (at center) are of argentic galena (PbS) (**gn**). The inclusions in sphalerite (light gray) are of arsenopyrite (see Fig. 9b).

Figure 10a. Sotiel complex sulfide ore, as mined (BEI). Magnified view of area W3 in Figure 9a. Detail of the fringes of argentic galena (PbS) (**gn**) (white) associated to arsenopyrite (FeAsS) (**apy**) and tetrahedrite ($\text{Cu}_3\text{Sb}_3\text{S}_4$) (**ttr**). Arsenopyrite shows submicroscopic inclusions of argentic galena, while galena is associated with aggregates of argentic tetrahedrite. The area with geometrical contour included in galena is composed of magnetite (FeFe_2O_4) (**mag**).

Figure 11a. Sotiel complex sulfide ore, as mined (BEI), magnified view of area W4 in Figure 10b. Details of previous image, where it is possible to see white submicroscopic aggregates to the boundaries of galena (PbS) (**gn**) of uncertain definition and galena-tetrahedrite ($\text{Cu}_3\text{Sb}_3\text{S}_4$) (**ttr**) associations.

Characterization of Complex Sulfide Ores



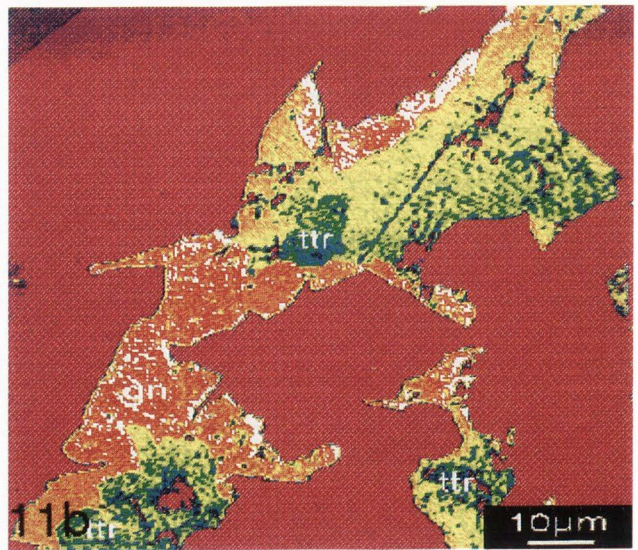
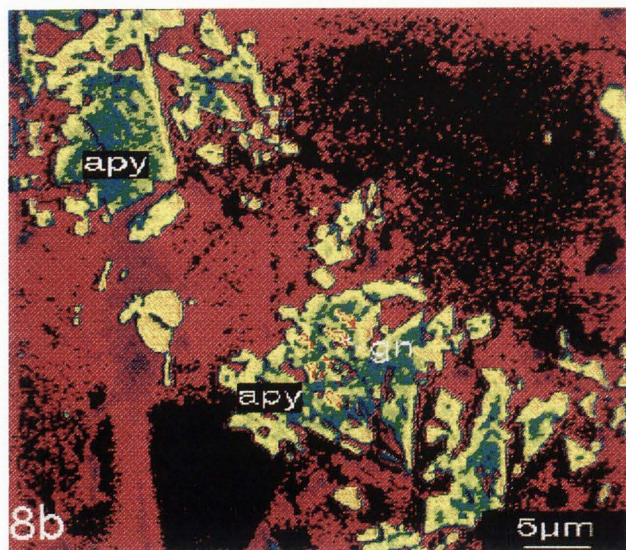
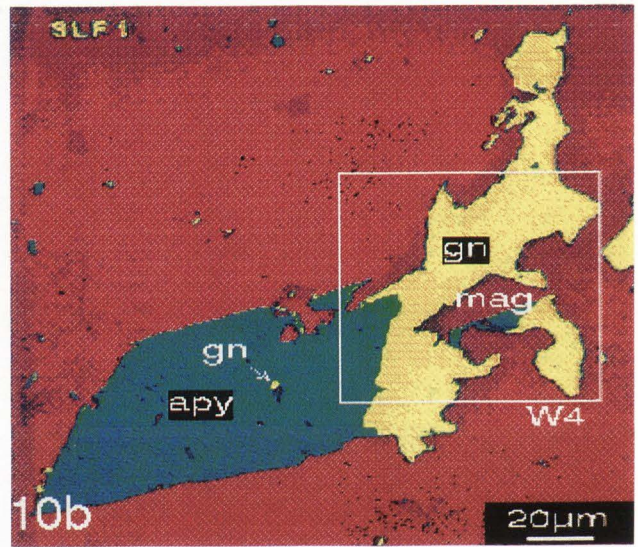
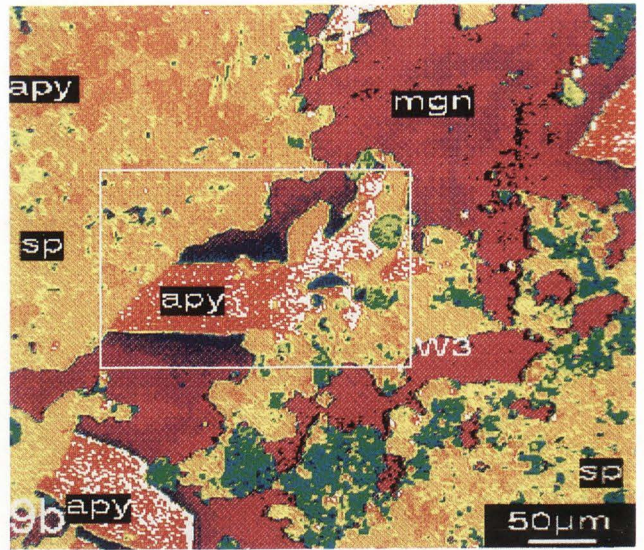
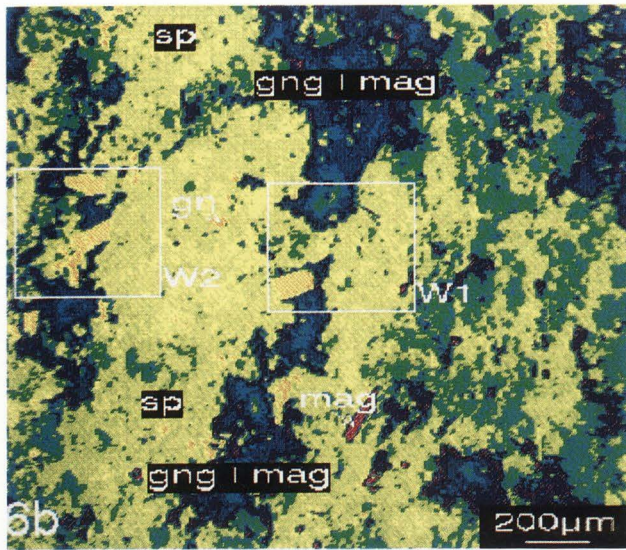


Figure 6b. Sotiel complex sulfide ore, as mined (digital topologic map, DTM). Note the different mineralogical species constituting the sample data detected in Figure 6a. The complex texture of the associations is evident. Microinclusions of aggregates of galena (PbS) (**gn**) can be detected. The sample is characterized by porosity and intergranular blowholes filled with magnetite (FeFe₂O₄) (**mag**) and gangue minerals (**gng**) (carbonate-quartz). The two windows plotted are representative of two different areas further magnified: W1 in Fig. 7; and W2 in Fig. 9).

Figure 7b. Sotiel complex sulfide ore, as mined (DTM). Note the different mineralogical species constituting the sample area described in Figure 7a. The different regions identified and labeled are representative of arsenopyrite (FeAsS) (**apy**). Some of the morphological and morphometrical aspects derived from the analyses are reported in the below.

Number of arsenopyrite (FeAsS) domains recognized and identified inside the sphalerite (ZnS) (number of Domains = 180).

Measure	Min	Max	Range	Sum	Mean	S.D.
Area	10	5015	5005	22529	125.2	438.9
Perimeter	10	952	942	8953	49.7	94.6
Roundness	1	14	13	414	2.3	2.1
Maj.Ax.	5	169	164	2578	14.3	16.9
Min.Ax.	2	42	40	1080	6.0	6.8

The *Area* and the *Perimeter* are expressed in pixels (1 pixel = 1.25 μm). S.D. = Standard deviation.

 Microanalyses of the gudmundite crystal (FeSbS) (white) reveal the composition of this phase (see Fig. 7c).

gudmundite (FeSbS), Ag-tetrahedrite (Cu₃Sb₃S₄), magnetite (FeFe₂O₄), marcasite (FeS₂) melnikovite, antimonite (SbS₃), cassiterite (SnO₂), and native bismuth. Rock seems to have a bright yellow color which contrasts with the dark-gray color of the background for the presence of massive pyrite.

Pyrite (FeS₂) is the most representative mineral occurring in granular, subautomorphic forms with regular crystals characterized by isodiametric "habitus", and with framboid or spheroidal structure or in former zone-concentric colloform growths. It has the highest inclusion content in association with sphalerite, galena, and chalcopyrite which cause very solid aggregate formation with very few vacuolar micro-blow-holes and total absence of microfracture systems or discontinuities (Fig. 2). The XRMA data on different areas of subauto-

Figure 8b. Sotiel complex sulphide ore, as mined (DTM). Pointed out the presence of galena (PbS) (**gn**) inside the arsenopyrite (FeAsS) (**apy**) recognized in Figure 8a. The different regions identified and labeled are representative of galena. Some of the morphological and morphometrical aspects derived from the analyses are reported below.

Number of galena (PbS) domains recognized and identified inside the arsenopyrite (FeAsS) (number of domains = 6).

Measure	Min	Max	Range	Sum	Mean	S.D.
Area	12	112	100	383	63.8	37.6
Perimeter	11	49	38	190	31.7	13.6
Roundness	1	2	1	8	1.3	0.3
Maj.Ax.	5	19	14	75	12.6	4.9
Min.Ax.	3	8	5	36	6.1	1.9

The *Area* and the *Perimeter* are expressed in pixels (1 pixel = 0.125 μm). S.D. = Standard deviation.

 Micro-analyses of the arsenopyrite (FeAsS) crystals reveal the composition of this phase (see Fig. 8c).

Figure 9b. Sotiel complex sulfide ore, as mined (DTM). Note the presence of different mineral species. The window plotted (W3) has been further magnified and analyzed in Figure 10. Microanalyses of arsenopyrite (FeAsS) (**apy**) and magnetite (FeFe₂O₄) (**mgn**) reveal the composition of these phases (see Fig. 9c and 9d, respectively).

Figure 10b. Sotiel complex sulfide ore, as mined (DTM). Increasing the magnification, further details and microstructures become "visible". The area identified as W4 has been further magnified and analyzed in Figure 11.

Figure 11b. Sotiel complex sulfide ore, as mined (DTM). Different mineralogical species constituting the microstructure are pointed out.

 morphic or relict or relict-fragmentary phases of pyrite show traces of As, Co, Cu (Table 2). In the clastic lithologic type, the XRMA data on different areas of subautomorphic or relict-fragmentary phases, neither showed appreciable amounts of nickel, cobalt or other elements, nor the presence of colloform or metacolloidal growth textures.

Sphalerite (ZnS) is detectable only through optical microscope reconnaissance because of its inner reddish-brown reflexes which are very marked especially at the edges of vacuolar micro-blow-holes which often characterize this mineral (Fig. 1). It shows heterogranular structure, irregular contour, and in some places either intertwined or in very small aggregates as substitution product. The marmatitic variety rich in Fe (ZnS), always present in this mineral, seems to be bound to

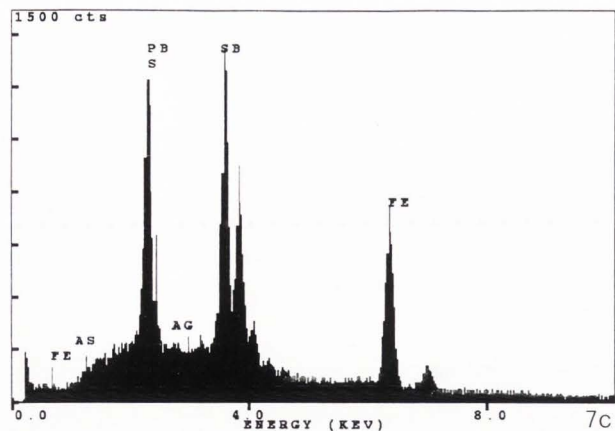


Figure 7c. Microanalysis of the gudmundite (FeSbS) (*gdm*) crystal shown in Figure 7b.

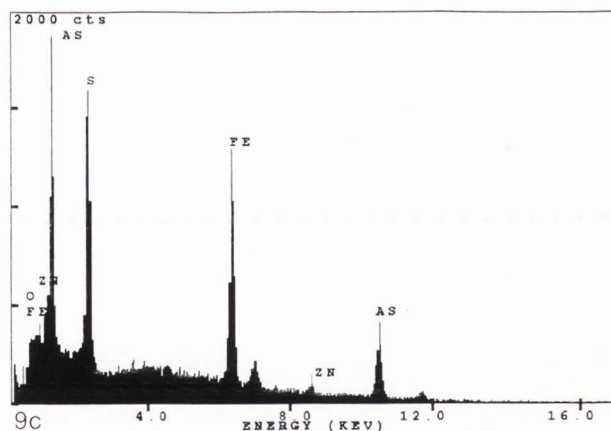


Figure 9c. Microanalysis of the arsenopyrite (FeAsS) (*apy*) crystal shown in Figure 9b.

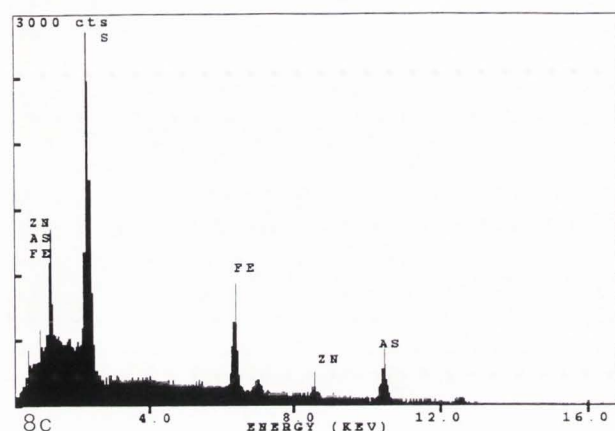


Figure 8c. Micro-analysis of the arsenopyrite (FeAsS) (*apy*) crystal reported in Figure 8b.

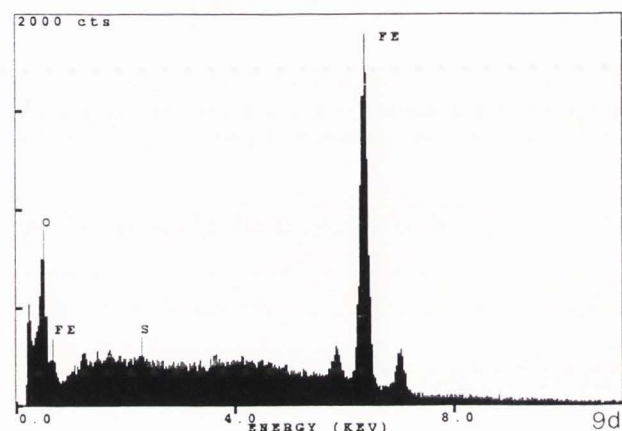


Figure 9d. Microanalysis of the magnetite (FeFe_2O_4) (*mag*) crystal shown in Figure 9b.

complex formation including those of substitutions in gangue minerals such as quartz and carbonate (Fig. 5). Sphalerite occurs as host mineral inside chalcopyrite (Fig. 4); chalcopyrite occurs either by itself or is observed in the shape of cord (bead) exsolutions, often broken by magnetite. Sphalerite is widespread as inclusions in galena (PbS), arsenopyrite (FeAsS) and tetrahedrite.

Galena (PbS) is found mainly in small aggregates and similar to sulfide of hypogenic formation, it tends to replace and include the metallic minerals of ancient formation such as sphalerite (ZnS), pyrite (FeS_2), and those of gangue, such as, quartz (SiO_2) and carbonate (Fig. 3).

Chalcopyrite (CuFeS_2) is similar in behavior to galena (PbS); it is found by itself or in the shape of cord (bead) exsolutions in sphalerite, galena, marcasite (FeS_2) and tetrahedrite ($\text{Cu}_3\text{Sb}_3\text{S}_4$) (Figs. 3 and 4).

Arsenopyrite (FeAsS) is the most widespread of the inferior mineralogical species. Under the microscope, it is characterized by a high reflectance and bright white color when it grows together with pyrite, while granular or subautomorphic intergrowth in sphalerite is easily detected by its yellow-pink colors and evi-

dent anisotropic characteristics (Fig. 3). Submicroscopic inclusions in pyrite and sphalerite are very clear under the electron microscope (Figs. 7 and 8). XRMA permits a better characterization of arsenopyrite both from a textural and morphological point of view (Figs. 6, 9 and 10), showing the strong intergrowth of this specie with others (as tetrahedrite and galena) (Fig. 11) not recognizable by optical microscopy.

Tetrahedrite ($\text{Cu}_3\text{Sb}_3\text{S}_4$) is present with tennantite (analyzed through XRMA) and is of argentic type with arsenic content below the detectability limit (Table 2). It always occurs in combination with galena and gudmundite. It grows together with other sulfides and primary oxides such as pyrite, sphalerite and magnetite (Fig. 11). Under the microscope, it has the typical olive-gray color with a lower reflectance than galena and higher reflectance than sphalerite. At crossed nicols, it shows perfect isotropy with complete extinction.

Gudmundite (FeSbS) under the microscope, shows clear diagnostic character despite its reflectance being very similar to that of arsenopyrite. Its white

color, with a trace of pink, is particularly clear in oil dipping. Its anisotropy, with more colored tones, and weak development towards idiomorphism, are the characters that distinguish it from arsenopyrite.

Quartz (SiO₂) is one of the most widespread constituents of gangues in the mineral of Sotiel. It is found in massive granular aggregates, of precocious generation, often replaced with metallic minerals or carbonate (Ankeritic Dolomite). Under the microscope, it shows common optical characters: its lower reflectance than sphalerite is a good discriminant criterion during image analysis. Its morphological relationships with metallic minerals are different, but in general, quartz grains are cemented to each other as well as with other minerals.

Carbonate is composed of ankeritic dolomite [CaMg(CO₃)₂ - CaFe(CO₃)₂] and like quartz, it is a well represented gangue mineral. It shows granular structure with pigmentation areas of brown and ochraceous tones, probably due to the presence of variable iron hydroxide concentrations (more than 10%).

Chlorite, a gangue mineral with secondary genesis, is found very frequently and exclusively combined with quartz, carbonate, magnesite, and oxides of Fe, especially in vacuolar micro-blow-holes which characterize the massive lithologic type. In thin section, it is green, and in some places reddish-brown. Its identification through the optical microscope, is very difficult because of its small crystal size. Yet, its typical structure is vermiform, and from the XRM data for its Fe content, chlorite is rich in Fe (more than 30%).

Discussion

The morphological aspects, correlated with XRM data, lead to the following:

In the ore, pyrite (FeS₂) is the most widespread phase present as microscopic (15-50 μm) and sub-microscopic inclusions (< 15 μm) in sphalerite (ZnS), galena (PbS), and chalcopyrite (CuFeS₂). In its granular or subautomorphic state, As, Co, and Cu are present, while Ni, Ag, and Au are below the detectability limit; in the schistose lithologic type, the framboid-spheroidal pyrite shows a regular chemical behavior. As and Bi are present in variable proportions, while Sb and Au are below the detectability limit.

Sphalerite is made up of crystalline microgranular aggregates with heterodiametric contour. Basic characteristic of this sulfide, apart from the abundance of residual pyrite, is the abundance of inclusions or exsolutions of galena, chalcopyrite, and arsenopyrite (FeAsS). The data in the Table 2, show a high Fe content (> 4%) for sphalerite, thus it can be considered a iron-rich sulfide (marmatite).

Galena, never idiomorphic, similar to minerals of late hypogenic formation, fills the corrosion pockets of pyrite, sphalerite, and gangues with very ancient formation. It shows a normal chemical behavior with silver content recoverable from the economic point of view.

Chalcopyrite shows a behavior similar to that of galena, it is found by itself or as exsolution in sphalerite.

Tetrahedrite (Cu₃Sb₃S₄) and gudmundite (FeSbS) are argentic; despite the fact they belong to the inferior species, these are present in all samples examined, except for those belonging to schistose lithologic type. They occur in small amounts.

Conclusions

Different minerals and/or their associations have been investigated in Sotiel ore. The experimental results and their interpretation can be summarized as follows:

Residual pyrite (FeS₂) with microscopic inclusions in very fine intergrowth of galena (PbS), chalcopyrite (CuFeS₂) or relict forms of marmatitic sphalerite (ZnS) (< 15 μm) have been detected.

Microcrystalline sphalerite in small patches or substitution zones in the granular and automorphic pyrite, granulations or cryptocrystalline expressions in arsenopyrite (FeAsS), and in chalcopyrite has also been pointed out, together with exsolutions of chalcopyrite, galena and arsenopyrite in sphalerite.

Microassociations of chalcopyrite-sphalerite in marcasite (FeS₂) and submicroscopic inclusions of Ag-galena in arsenopyrite and associations with Ag-tetrahedrite (Cu₃Sb₃S₄) and Ag-gudmundite (FeSbS) have been revealed.

Associations of marcasite-melnikovite-antimonite and magnetite-mineral of gangue (quartz-ankeritic dolomite, chlorite) together with associations of cassiterite-galena-sphalerite and native bismuth in the residual pyrite have also been recognized.

On the basis of these results, the mineralization shows genetically a very complex nature, in relation of a sulfide mineralization.

The microstructural characterization realized by SEM techniques and image analyses enabled to realize a complete topological assessment of the different mineralogical species constituting the ore. This information is of particular interest to define and set up suitable models of liberation for the species of interest in order to operate a preliminary selection on the process (i.e., comminution circuit) and the parameters (i.e., size class ranges) to realize the maximum recovery. Furthermore, the proposed approach enables us to reach an other very important goal, strictly linked with the use and the process of digital information: the construction of data-bases to consult, as an historical memory, during any further characterization of the same or other ores presenting similar characteristics.

Acknowledgments

The authors wish to thank Dr. Eng. G. Belardi and Dr. P. Plescia of Istituto per il Trattamento dei Minerali, C.N.R. for their cooperation during some of the analytical studies.

References

- Apps A (1961). An account of the geology, petrology and mineralogy of San Miguel concession and ore bodies of the Province of Huelva, Spain. Thesis. Royal School of Mines. Imperial College, London, England.
- Arnold M, Soler E (1973). Le minéralisations pyriteuses associées au vulcanisme quartz-kératophyrique du Sud de la Péninsule Ibérique (The pyritic mineralizations associated with quartz-cheratophiric volcanism in the South of Hiberian peninsula). *C. R. Acad. Sc. Paris* **276(D)**: 1373-1376.
- Bard JP (1965). Introduction à la géologie de la chaîne hercynienne dans la Sierra Morena occidentale (Espagne). Hypothèse sur les caractères de l'évolution géotectonique de cette chaîne {Introduction to the geology of the hercynian chain in the West of Sierra Morena (Spain). Hypothesis on the evolution characteristics}. *Rev. Geogr. Phys. et Geol. Dyn.* **7**: 323-337.
- Bonifazi G, Massacci P (1986). Mineral recognition and degree of liberation measurements in industrial ore processing: Scanning Electron Microsc. **1986**;I: 117-128.
- Bonifazi G, Massacci P (1988). Description of a breakage function by image processing. Proceedings of: XVIth International Mineral Processing Congress, Stockholm (copy available from G. Bonifazi).
- Bonifazi G, Massacci P (1989). An approach for evaluating a liberation function by image processing. Proceedings of MMIJ/IMM Joint Symposium on Today's Technology for the Mining and Metallurgical Industries, Kyoto, Japan (copy available from G. Bonifazi).
- Delcey R. (1970). Notes sur la stratigraphie et le volcanisme de la Province pyrito-cuprifère du Baixo-Alentejo, Portugal (Notes on the stratigraphy and the volcanism of Baixo-Alentejo pyrite province, Portugal). *Estudios Notas e Trabalhos do Servios de Fomento Mineiro*, **19** (3-4): 199-225, Porto, Portugal.
- Febrel T. (1967). Estratigrafia, tectónica y petrografia de la zona di Calanas (Huelva) {Stratigraphy, tectonics and petrography of the Calanas (Huelva) area}. E.N.A.D.I.M.S.A., Madrid. Copy available from Minas de Almagrera, Grupo Minero Sotiel-Calanas, Huelva, Spain.
- Febrel-Molinero DT (1966). Notice explicative de la carte géologique au 1/50.000x de Calanas (Huelva), Espagne {Explicative notes of the geological map (1: 50.000) of the Calanas (Huelva) area}. Copy available from Minas de Almagrera, Grupo Minero Sotiel-Calanas, Huelva, Spain.
- Fernandez A (1975). Los yacimientos de sulfuros polimetálicos de S.O. Iberico y sus metodos de prospeccion (South-West spanish polymetallic sulphide ores characterization and investigation). *Studia Geol. Universidad de Salamanca, Spain.* **9**: 65-102.
- Garcia Palomero F (1974). Caracteres estratigraficos del anticlinal de Rio Tinto {Rio Tinto (Spain) anticlinal stratigraphic characteristics}. *Studia Geol. Universidad de Salamanca, Spain.* **8**: 93-124.
- Gorga R (1989). Grain size distribution of a Greek Pb-Zn sulphide ore by image analysis. *Ind. Mineraria* **6**: 1-10.
- Kinkel AR Jr (1962). Observation on the pyrite deposits of Huelva (Spain) and their relations with volcanism. *Econ.Geol.* **57**: 1071-1080.
- Lecolle M (1970). Note préliminaire sur le métamorphisme et la tectonique de la Province pyrito-cuprifère d'Huelva (Espagne). Conséquences pétrologiques {Preliminary notes on the Huelva (Spain) pyrite-copper province metamorphism and tectonic. Petrographic consequences}. *C. R. Acad. Sc. Paris* **270(D)**: 1563-1566.
- Lecolle M (1971). Séquence lithostratigraphique dans la Province d'Huelva: position des minéralisations manganésifères et pyriteuses (The lithostratigraphic sequence of Huelva province: manganese and pyrite minerals). *C. R. Ac. Sc. Paris* **272(D)**: 1956-1959.
- Lecolle M (1972). Successions lithologiques et stratigraphiques dans la province d'Huelva: position des minéralisations manganésifères et pyriteuses (Huelva province lithologic and stratigraphic sequence: manganese and pyrite minerals). *C. R. Ac. Sc. Paris* **274(D)**: 505-508.
- Lecolle M, Roger G (1973). Métallotectes lithostratigraphiques et paléogéographiques dans la province pyrito-cuprifère sud-Ibérique (Metallotectonic, lithostratigraphic and paleogeographic characteristics of the South Spanish pyritic-copper province). *C. R. Ac. Sc. Paris*, **276(D)**, 141.
- Petruk W (1986). Predicting and measuring mineral liberation in ores and mill products, and effect of mineral textures and grinding methods on mineral liberation. In: *Process Mineralogy VI*. Hagni RD (ed.). Am. Inst. Mining Metallurg. Eng., The Metallurgical Society (AIME/TMS), Warrendale, PA. 393-403.
- Petruk W (1988). Ore characteristics that affect breakage and mineral liberation during grinding. In: *Process Mineralogy VIII*. Carson DJT, Vassiliu AH (eds.). AIME/TMS, Warrendale, PA. 181-193.
- Petruk W (1990). Measurements of mineral liberation in connection with mineral behaviour. In: *Process Mineralogy IX*. Petruk W, Hagni RD, Pignolet-Brandom S, Hausen DM (eds.). AIME/TMS, Warrendale, PA. 31-36.
- Rambaud F (1969). El sinclinal Carbonifero de Rio Tinto y sus mineralizaciones asociadas (Rio Tinto coal sinclinal area and its mineralizations). *Mem. I. G. M. E.* **71**. Copy available from Minas de Almagrera, Grupo Minero Sotiel-Calanas, Huelva, Spain.
- Schermerhorn L (1971). On outline stratigraphy of the Iberian Pyrite Belt. *Bol. Geol. y Min. Madrid* **82(3/4)**: 239-268.
- Soler E. (1971). Observations préliminaires sur la province métallogénique de Huelva. Stratigraphie et tectonique (Preliminary observations on Huelva metallogenic province. Stratigraphy and tectonic). *C. R. Ac. Sc. Paris* **272(D)**, 1197-1200.

Discussion with Reviewers

N.K. Tovey: You indicate that you lapped the surfaces with increasingly fine powders down to 5 μm . Many other laboratories use even finer paste. Did you try this, and if so, does this give a better final surface?

Authors: During sample preparation different polishing strategies were adopted, and also fine powders smaller than 5 μm were used. The results obtained in terms of the quality of resulting surfaces compared with the results of SEM analyses did not justify, in our opinion, the amount of time and cost to obtain an "high quality" polished section, taking into consideration the mechanical characteristics of the ore under study.

N.K. Tovey: You say that you used a home-made digitizing facility; could you please briefly say what this consisted of? I presume that the optical microscope images were digitized using a camera: was this a CCD? For the SEM images, did you digitize the signal directly, or obtain the digital images from photographs? What pixel array did you use (i.e., 512 x 512 or another) and were these rectangular or square? Finally, what intensity resolution did you use (8 bit, 16 bit)?

Authors: The system utilized to acquire, handle, and process images consists of a simple "frame grabber" able to freeze a pixel array of 512 x 512 pixels (from 8 to 24 bits per pixel). The optical microscope images were digitized using a CCD color camera (i2s 800CC). For SEM images, we acquired them from photographs or better negatives (Polaroid film) using a 5000°K source light and a CCD black and white camera (Sony AVC-D5CE). The SEM images, starting from negatives, were acquired using a 512 x 512 rectangular pixel array (4:3 ratio), the intensity resolution was 8 bit.

N.K. Tovey: It is not entirely clear, but I presume that you overlaid optical images with those from SEM, and/or microprobe. You indicate that you used multi-correlation techniques: I presume that here you refer to the correlation between one spectral layer and another? However, if this is the case, then precise spatial correlation between the images from the different instruments is necessary. How did you achieve this? There seem to be two possibilities: first, by manual location of 3+ control points in all images, and second, by some form of spatial cross-correlation. Which did you use?

Authors: We overlaid optical, SEM, and microprobe images. Of course, such a procedure was not applied on the entire set of images analyzed during the study but only on a limited number in order to verify the possibility offered by such an approach. We applied multi-correlation techniques among the different spectral layers constituting the image samples, different well known strategies can be adopted and the results obtainable are strictly a function of the procedure utilized. The real problem in such a study, as well recognized in the question, is to find a suitable strategy for spatial correlation for images coming from different instruments, acquired for different periods of time and with different resolution characteristics. At this stage of the study, we adopted a combined system based on linear interpolation and a manual location utilizing different control points to realize a "perfect" overlay of the images. At the moment we do not think that a "direct" form of a spatial cross-correlation could be applied on images, due to the very marked differences between images coming from the different analytical systems previously mentioned.

N.K. Tovey: What do the numbers on Figures 2, 3 and 4 refer to?

Authors: The "numbers" on Figures 2, 3 and 4, are the "labels" associated with different regions constituted by sphalerite (Zns) (**sp**) for Figures 2 and 3, and pyrite (FeS_2) (**py**) for Figure 4. The identification of such a region is based on their spectral characteristics (RGB components). The procedure consists in evaluating such characteristics, to distinguish them from those of the other regions (mineral species) present in the same image, and to append to each pixel of the recognized domain a label number. This way further morphological and morphometrical evaluation is much simplified.

Editor: Please give details on the paper by Bonifazi and Gorga (submitted for publication).

Authors: Bonifazi G, Gorga R (1993). Structural and textural characterization of Sotiel complex sulphide ore (South of Sierra Aracena, Spain) by optical and digital analysis. Submitted for publication to: Economic Geology.